J. Fluid Mech. (2023), *vol*. 959, A12, doi:10.1017/jfm.2023.136

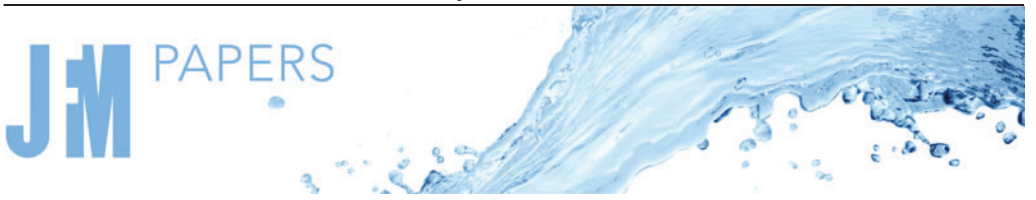

Hemline breakup of gel drops subjected to a continuous air flow

Zi-Yu Wang[1], Feng Yao[2], Hui Zhao[1],†, Zhe-Hang Shi[2] and Hai-Feng Liu[1]

[1]National Energy Coal Gasification Technology Research and Development Center, Shanghai Engineering Research Center of Coal Gasification, East China University of Science and Technology, Shanghai 200237, PR China

[2]Shanghai Engineering Research Center of Space Engine, Shanghai Institute of Space Propulsion, Shanghai 201112, PR China

(Received 25 July 2022; revised 9 January 2023; accepted 11 February 2023)

To explore the effect of yield stress on the secondary breakup of gel drops, experimental and theoretical investigations are carried out by employing a high-speed camera. A unique hemline-type breakup, as a modified behaviour of sheet-thinning breakup, occurs when the air velocity increases to a high region. The edges of the drops constantly deform into thin membranes when the high-velocity air skims over the gel drops. These membranes vibrate vertically, and breaking points occur at high amplitudes, causing the formation of reticular fragments. The results of linear stability analysis indicated that the yield stress of the gel drops has an influence on the formation and breakup of the gel membranes. The breakup regime map and breakup times are also studied.

Key words: aerosols/atomization, rheology

1. Introduction

Atomization has numerous applications in industrial processes such as spray combustion (Hoang 2021; Tuan Hoang & Viet Pham 2021; Wu, Zhang & Zhang 2021), medical technology (de Oliveira *et al.* 2021; Sharma *et al.* 2021) and the production of particles (Beckers *et al.* 2020; Wei *et al.* 2020). The atomization process is generally divided into two parts: primary atomization and secondary atomization. During the primary atomization process, the jet disintegrates into drops under the instabilities developed on the jet surface (Jiao *et al.* 2017). Secondary atomization is defined as these drops deform and break into tiny drops under the action of the aerodynamic force, viscous resistance and surface tension (Guildenbecher, López-Rivera & Sojka 2009). Increased surface area leads to improved mass and heat transfer rates as drops break up into smaller fragments, which contributes to the acceleration of the reaction. Therefore, secondary atomization is

† Email address for correspondence: zhaohui@ecust.edu.cn

of great importance in industrial processes. Many studies have been done via theoretical deductions, experiments and numerical simulations (Eggers & Villermaux 2008; Kékesi, Amberg & Prahl Wittberg 2014; Yang *et al.* 2016; Rimbert *et al.* 2020).

Conventionally, the secondary breakup of Newtonian fluids is divided into different breakup modes according to their morphologies and mechanisms: bag breakup, bag-stamen breakup, multimode breakup, sheet-thinning breakup and catastrophic breakup (Pilch & Erdman 1987; Hsiang & Faeth 1995; Dai & Faeth 2001; Guildenbecher *et al.* 2009). These breakup modes are categorized into two regimes: the Rayleigh–Taylor piercing (RTP) and the shear-induced entrainment (SIE), which are mainly governed by the Rayleigh–Taylor instability and the Kelvin–Helmholtz instability, respectively. The RTP is characterized by a flattened drop that deforms into a bag (or bag-stamen structure or bags), through which the air pierces and traverses (Zhao *et al.* 2010; Kulkarni & Sojka 2014). However, the internal flow mechanism suggests that the flow of the liquid dominates the droplet deformation process, which has been investigated through experiments and simulations. A three-step calculation based on the internal flow mechanism was proposed by Jackiw & Ashgriz (2021) to mathematically describe the realistic process of different breakup morphologies. Kant & Banerjee (2022) studied the deformation process of the droplet and the properties of the air-flow field around the droplet. The simulation results indicated that the recirculation zone in the air-flow field significantly influences the pressure distribution on the surface of the droplet, leading to the interior shift of liquid in the droplet and the deformation of the droplet. In SIE, the unstable waves develop near the equator, causing the formation of ligaments and fragments at the edges while the frontal area remains smooth (Kékesi, Amberg & Prahl Wittberg 2016; Zhu *et al.* 2021). The secondary breakup process of non-Newtonian fluids drop has been investigated in many studies. Minakov *et al.* (2019) performed a series of detailed numerical simulations to explore the influence of the Weber number *We* on the secondary breakup of Bingham fluids. They obtained the transitional *We* between different breakup modes and investigated the temporal evolution of the ratio of the cross-steam diameter to the initial diameter. Using numerical simulations, Chu *et al.* (2020) studied the bag breakup behaviour of polymer solutions considered to be Herschel–Bulkley fluids. Unlike Newtonian fluids, a reticular structure appeared during the bag breakup of the polymer drops. They also established a formula to calculate the transient drag coefficient during bag breakup based on the cross-steam diameter of the drops. In the study of Qian *et al.* (2021), carboxymethyl cellulose (CMC) solution drops were described by the power-law rheological model. They found that the liquid ring remained after bag breakup, which may be related to the enhanced stability of the drops due to the CMC polymer chains.

In recent years, gels have been increasingly applied in the food industry (Cao & Mezzenga 2020), medical technology (Narayanaswamy & Torchilin 2019; Daly *et al.* 2020) and fuels and propellants (Glushkov, Pleshko & Yashutina 2020; Padwal, Natan & Mishra 2021; Glushkov *et al.* 2022). The commonly used gels are mostly polymers, whose long-chain molecular structures form strong entangled or cross-linked networks through hydrogen bonds when dispersed in water. Therefore, gels have unique properties such as thickening, stabilizing, binding, etc. Gels exhibit shear-thinning behaviour when the shear stress is higher than the yield stress. The yield stress is a critical property of the gel and the reason for its resistance to small perturbations. Inspired by the above references and the complex rheological properties of gels, we conducted an experimental investigation on the secondary breakup process of gel droplets. A high-speed camera was used to obtain the images of gel drop deformation and breakup. The breakup morphology, breakup time and the effect of yield stress on secondary breakup are studied in this article.

	Concentration φ (mass fraction)	σ_l (mN m^{-1})	ρ_l (kg m^{-3})
Gel	0.5 %	60.0	958.7
	1.0 %	52.8	964.8
	1.5 %	50.9	989.6
maltose syrup	70 %	57.6	1262.8

Table 1. Physical properties of guar gum gels and maltose syrup.

2. Experimental set-up

The guar gum gels used in the secondary atomization experiment were water-based gel simulants. We prepared a series of gels of different mass concentrations φ by dissolving guar powder in ultrapure water. The guar gum–water solutions rested until completely dissolved. After that, a blender was used to stir them for at least 30 min. Before the secondary atomization experiments, the guar gum gels were allowed to stand at room temperature for 3 hours to remove air bubbles. We measured the surface tension of guar gum gels by the Wilhelmy plate method and repeated the experiments three times to ensure repeatability. The result was the average of these three experiments. The rheological properties of the guar gum gels were measured by a rotational rheometer (Bohlin CVO Rheometer, Malvern Instruments). The experiments were repeated three times to ensure repeatability. The physical properties of guar gum gels are listed in table 1. Maltose syrup was used for controlled trials, and its physical properties are also listed in table 1.

The schematic of the experimental apparatus was identical to our earlier work (Zhao *et al.* 2010, 2011*b*), as shown in figure 1. The droplet generator was composed of a gel tank and a small diameter tube fixed at the bottom of the tank. At the exit of the tube, a gel droplet formed and fell into a continuous and uniform air-flow field. A circular nozzle combined with a root blower generated the air-flow field measured by a high accuracy rotameter. The internal diameter of the air nozzle was 68 mm, and the horizontal distance between the initial droplets and the air nozzle was 15 mm. The mean air velocity and the root mean square air velocity profile were measured by Dantec hot-wire anemometry in our earlier work (Zhao *et al.* 2010). According to the measurement, the droplets entered the core-flat area of the air jet flow. Therefore, the influence of the boundary layer can be ignored since the boundary layer is thin. A high-speed camera (Fastcam SA2, Photron,) was used to capture the droplet entering the air-flow field and breaking up under the shear of high-speed air. The frame rate was higher than 2000 images per second. The resolution of the pictures was higher than 1024×1024 pixels. The physical resolution of images of the gels and the maltose syrup is 206.19 μm pixels^{-1}. We experimented at atmospheric pressure and room temperature. The digital photo images were measured with the NIH IMAGE software. The measurements were repeated three times to ensure repeatability, and the results were the average of the three experiments.

3. Result and discussion

3.1. *Dimensionless groups*

The secondary breakup of Newtonian fluid drops is resisted by the aerodynamic force, viscous stress and surface tension. Dimensionless numbers are applied to describe the competition between these different forces. The Weber number, *We*, is defined as the ratio

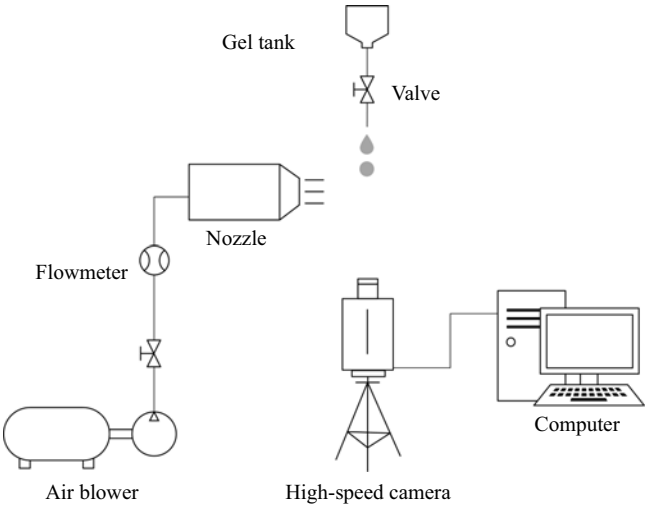

Figure 1. Schematic of the secondary atomization experimental apparatus.

of aerodynamic force to surface tension, representing their relative magnitude:

$$We = \frac{\rho_g u_g^2 D_0}{\sigma}, \tag{3.1}$$

where ρ_g and u_g are the density and the velocity of air, respectively, D_0 is the initial diameter of the drop and σ is the surface tension of the working fluid. For Newtonian fluids, the effect of viscosity on the atomization process is generalized by the Ohnesorge number, Oh:

$$Oh = \frac{\mu_l}{(\rho_l D_0 \sigma)^{1/2}}, \tag{3.2}$$

where ρ_l and μ_l are the density and the viscosity of the working fluid, respectively.

The rheological measurements of the guar gum gels are shown in figure 2. Shear-thinning behaviour was observed, where the viscosity decreased with increasing shear rate. Meanwhile, the yield stress was also observed during the rheological measurements. The shear-thinning properties and yield stress of the guar gum gels can be approximated by the Herschel–Bulkley rheological model, and it is

$$\tau(\dot{\gamma}) = \tau_0 + K\dot{\gamma}^n, \tag{3.3}$$

where the τ_0 is the yield stress, $\dot{\gamma}$ is the shear rate, K is the consistency and n is the fluid behaviour index. The experimental results were fitted to (3.3) over a range of shear rates from 1 to 400 s^{-1}, and the fitted results are listed in table 2 and plotted in figure 2. As shown in figure 2, the apparent viscosity of maltose syrup at a concentration of $\varphi = 70\,\%$ is 0.723 Pa s. We also tested the viscoelasticity of the gels that were used in our experiment with the rotational rheometer, as shown in figure 2(*c*). In general, the storage modulus G' characterizes the elastic properties of a material, while the loss modulus G'' characterizes the viscous properties. The elasticity of the gel of $\varphi = 0.5\,\%$ is too small and beyond the measurement range of the rotational rheometer, which means it can be considered negligible. Therefore, only G' and G'' of the gel of $\varphi = 1.0\,\%$–$1.5\,\%$ are obtained and shown in figure 2(*c*). For the gel with $\varphi = 1.0\,\%$, G' is initially smaller

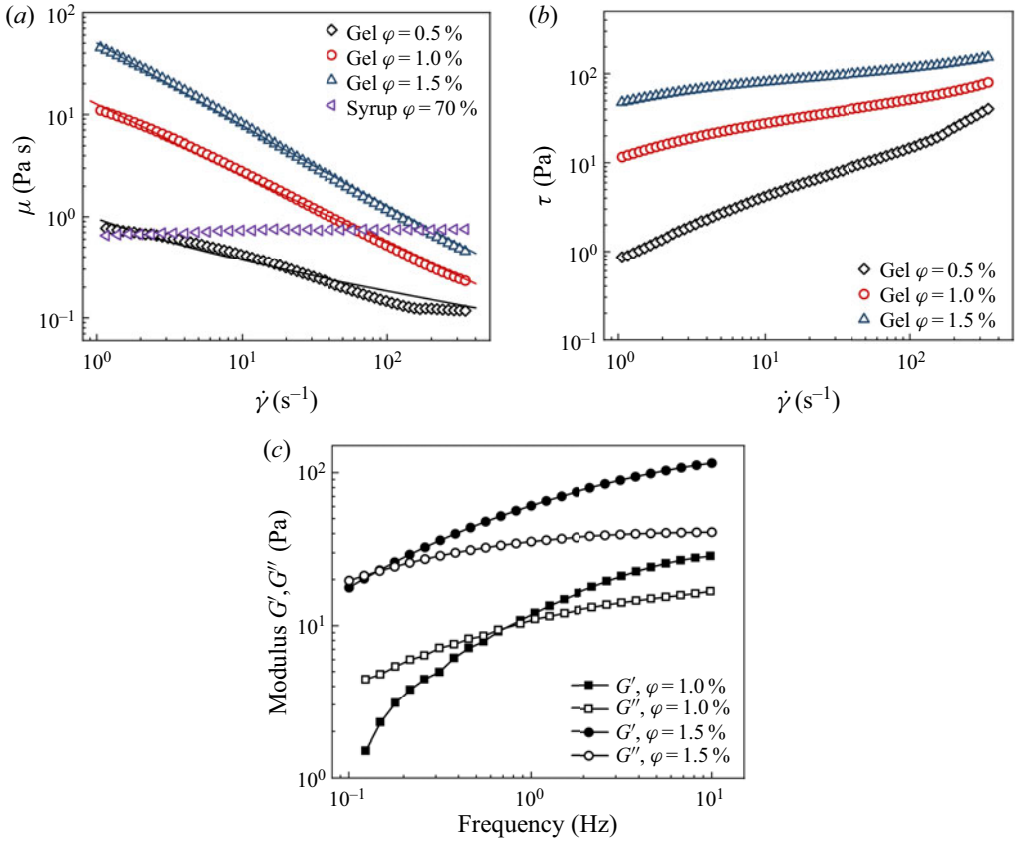

Figure 2. Rheological property measurements, (*a*) apparent viscosity μ vs. shear rate $\dot{\gamma}$; (*b*) shear stress τ vs. shear rate $\dot{\gamma}$; (*c*) viscoelastic measurements.

Suspension of different φ	τ_0 (Pa)	K (Pa s^n)	n
0.5 %	0.33	0.63	0.73
1.0 %	2.12	10.47	0.35
1.5 %	12.51	37.66	0.24

Table 2. Rheological properties of guar gum gels.

than G''; G' becomes larger than G'' when the frequency is higher. In other words, the gel with $\varphi = 1.0\,\%$ behaves as a viscous fluid at low frequencies and an elastic fluid at high frequencies. For the gel with $\varphi = 1.5\,\%$, G' exceeds G'' at first, which means the gel of $\varphi = 1.5\,\%$ behaves as an elastic fluid at most frequencies. The elasticity of the gel increases with increasing concentration.

The shear rate $\dot{\gamma}$ in the secondary atomization is usually defined as

$$\dot{\gamma} = \frac{\phi u_g}{D_0}, \tag{3.4}$$

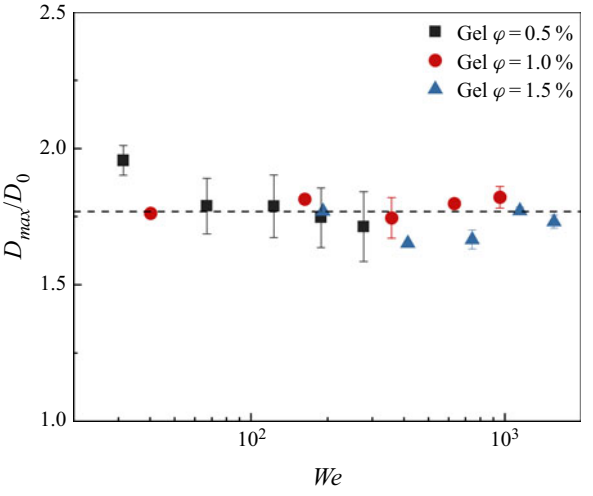

Figure 3. Values of D_{max}/D_0 of guar gum gel drops.

where ϕ is a coefficient. Therefore, Oh can be expressed as

$$Oh = \frac{\mu_l}{(\rho_l D_0 \sigma)^{1/2}} = \frac{\tau_0 + K\left(\phi \frac{u_g}{D_0}\right)^n}{\phi u_g \left(\frac{\rho_l \sigma}{D_0}\right)^{1/2}} = \frac{1}{\phi}\frac{\tau_0 D_0}{\sigma}\sqrt{\frac{\rho_g}{\rho_l We}} + \frac{K\left(\phi \frac{u_g}{D_0}\right)^{n-1}}{(\rho_l D_0 \sigma)^{1/2}}. \tag{3.5}$$

Based on the form suggested by Zhao *et al.* (2011*b*), (3.4) defines the shear rate on the surface of the droplets. The coefficient ϕ is a constant that describes the relationship between the velocity of the air-flow field and the shear rate on the surface of the droplet. As suggested by Zhao *et al.* (2011*b*), this coefficient is approximately $\phi = 2.9 \times 10^{-3}$. The value of Oh is obtained by inserting this coefficient.

3.2. *Morphological properties and breakup time*

Spherical gel drops fall into the air-flow field and deform into various shapes during the secondary atomization process. To quantifiably investigate the morphological properties of a gel drop during the process, D_{max}/D_0 was employed to describe the degree of deformation. Here, D_0 is the initial diameter of the gel drop and D_{max} is the maximum diameter of the gel drop after it is deformed into an oblate sheet. The D_{max}/D_0 values of gel drops are plotted in figure 3 against We, and the average of the D_{max}/D_0 values is approximately 1.77, as represented by the dashed line. As reported by previous researchers, the D_{max}/D_0 value of Newtonian fluids is approximately 1.75 (Zhao *et al.* 2011*a*; Yang *et al.* 2017). In the research of Dai & Faeth (2001) the value of D_{max}/D_0 of Newtonian fluids is 2.15. Considering that the viscosities of the working fluids they used (range of Oh is 0.0045–0.013) were much smaller than that of the working fluids in our experiment, it is acceptable that the D_{max}/D_0 value of our test is smaller. Zhao *et al.* (2014) studied the influence of the rheological properties of coal water slurry on the morphological properties during secondary atomization. the D_{max}/D_0 value of coal water slurry is approximately 1.47–1.76.

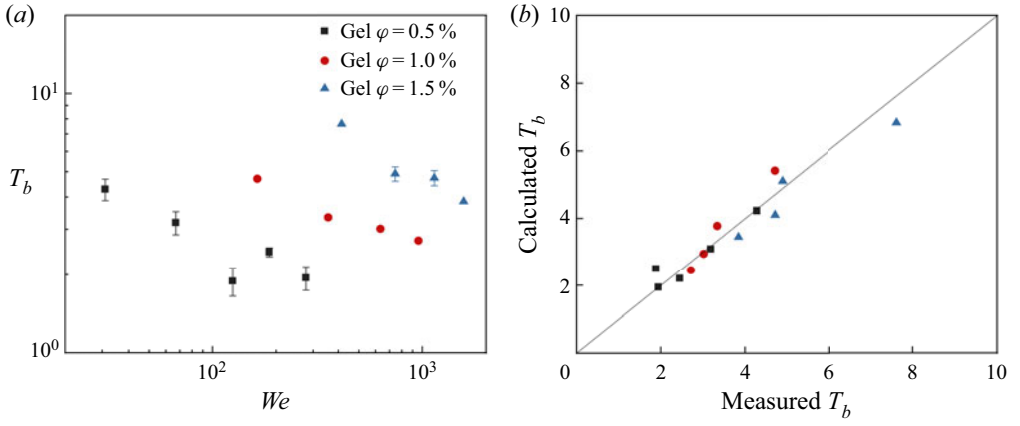

Figure 4. (*a*) Breakup time T_b of gel drop measured in secondary breakup; (*b*) comparison of measured T_b with calculated T_b.

The breakup time T_b is used to describe the secondary breakup process of gel drops, which can be represented as

$$T_b = \frac{t_b}{t^*} = \frac{t_b u_g}{D_0(\rho_l/\rho_g)^{1/2}}. \tag{3.6}$$

Here, t_b is the time from a spherical gel drop breaking into fragments, and t^* is the dimensional time of secondary breakup. The breakup times of different gels under different *We* values are shown in figure 4(*a*). The increase in *We* leads to a decrease in the breakup time due to the increase in aerodynamic force. The correlation of breakup time T_b of viscous droplets was given by Gelfand (1996), Pilch & Erdman (1987) and Guildenbecher *et al.* (2009). Combining these correlations, we fitted the breakup time T_b with dimensionless numbers *We* and *Oh*, and the result is

$$\begin{aligned} T_b &= 4.5(We-12)^{-0.25}(1+1.2Oh^{0.74}) \\ &= 4.5(We-12)^{-0.25}\left(1+1.2\left(\frac{1}{\phi}\frac{\tau_0 D_0}{\sigma}\sqrt{\frac{\rho_g}{\rho_l We}}+\frac{K\left(\phi\dfrac{u_g}{D_0}\right)^{n-1}}{(\rho_l D_0\sigma)^{1/2}}\right)^{0.74}\right), \end{aligned} \tag{3.7}$$

where the fitting correlation coefficient is 0.95. The calculated T_b values from (3.7) are plotted against the measured T_b in figure 4(*b*). Yield stress also affects the T_b value of gel drops. Increasing the yield stress leads to an increase in T_b, which is consistent with the experimental results.

3.3. *The breakup morphology*

Numerous studies have been conducted to explore the mechanism of secondary atomization of Newtonian fluid drops. In terms of the different breakup morphologies, the deformation and breakup modes of Newtonian fluid drops are classified into deformation (that means the drops will not break up), bag breakup (Theofanous & Li 2008; Theofanous *et al.* 2012), multimode breakup (also termed transition breakup) and shear breakup (also termed SIE) (Theofanous & Li 2008; Theofanous *et al.* 2012).

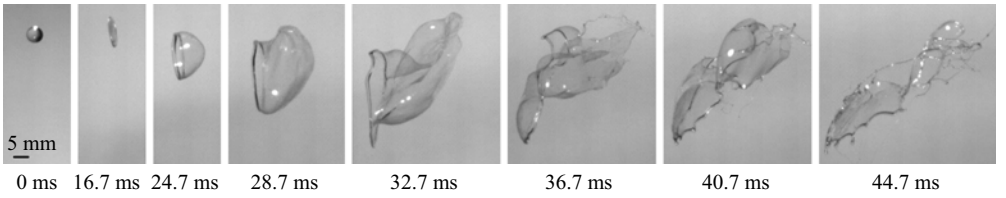

Figure 5. Bag breakup of the guar gum gel; the air flows from left to right ($\varphi = 0.5\,\%$, $u_g = 15.3\ \mathrm{m\ s^{-1}}$, $We = 31.3$, $Oh = 0.7$).

(*a*)

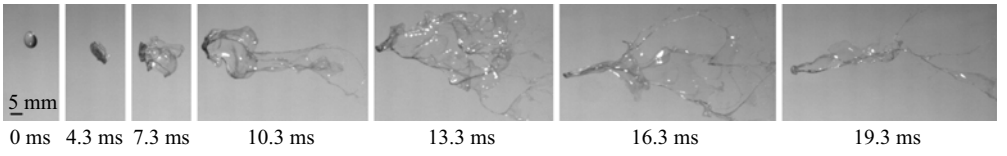

(*b*)

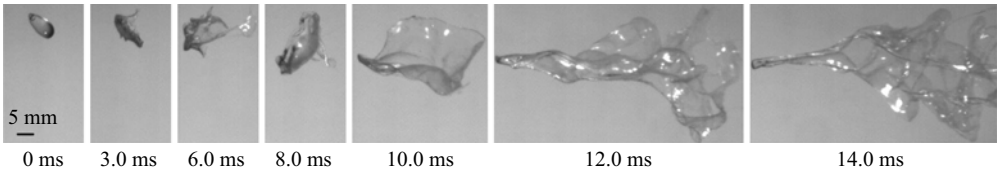

Figure 6. Stamen structure breakup of the guar gum gel; the air flows from left to right: (*a*) $\varphi = 1.0\,\%$, $u_g = 45.9\ \mathrm{m\ s^{-1}}$, $We = 357.8$, $Oh = 2.8$; (*b*) $\varphi = 1.5\,\%$, $u_g = 61.2\ \mathrm{m\ s^{-1}}$, $We = 736.1$, $Oh = 6.4$.

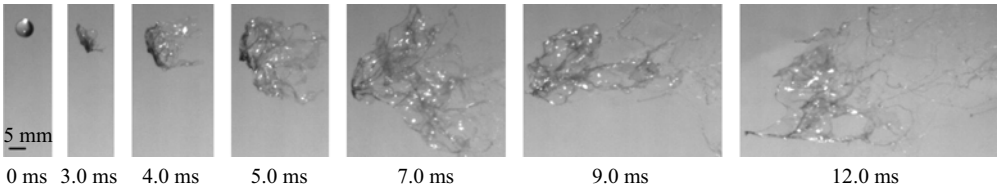

Figure 7. Hemline breakup of the guar gum gel; the air flows from left to right ($\varphi = 0.5\,\%$, $u_g = 45.9\ \mathrm{m\ s^{-1}}$, $We = 267.5$, $Oh = 0.5$).

The secondary breakup morphology of guar gum gel shows different breakup modes with the increase of air velocity, as shown in figures 5–9. The deformation regime appears when the air velocity is low. In this regime, the aerodynamic force is too small to take the dominant position, resulting in the absence of a breakup. The gel drop exhibits the bag-type breakup when the air velocity increases slightly, as shown in figure 5. A spherical drop initially flattens, then deforms into a bag-like structure and eventually breaks up during this regime. The stamen structures appear when the air velocity continues to increase. The drop initially deforms into a sheet, then the edges of the drop deform into thin membranes and ligaments. The core of the drop remains stable along the air flow, as shown in figure 6.

The gel drops enter the hemline breakup mode when the aerodynamic force dominates, as shown in figures 7–9. For Newtonian fluids, tiny fragments are continuously peeled off the drop surface in the shear breakup mode (Theofanous & Li 2008; Theofanous

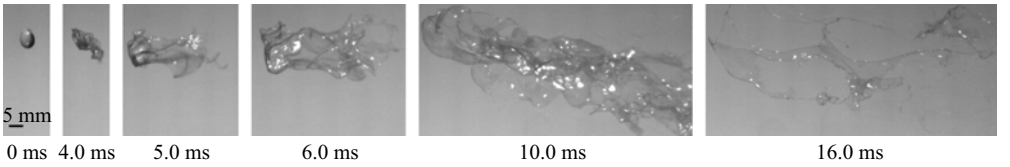

Figure 8. Hemline breakup of the guar gum gel; the air flows from left to right ($\varphi = 1.0\,\%$, $u_g = 76.5\ \mathrm{m\ s^{-1}}$, $We = 948.2$, $Oh = 1.9$).

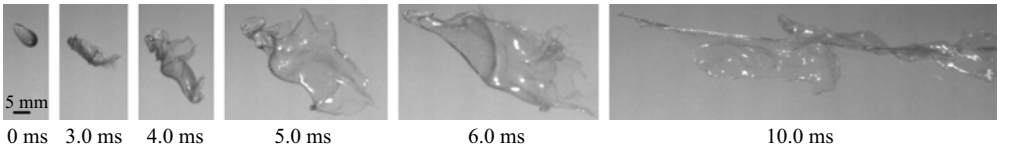

Figure 9. Hemline breakup of the guar gum gel; the air flows from left to right ($\varphi = 1.5\,\%$, $u_g = 91.8\ \mathrm{m\ s^{-1}}$, $We = 1560.6$, $Oh = 4.6$).

et al. 2012). Unlike Newtonian fluids, filaments rather than fragments form on the drop surface when an elastic drop undergoes secondary atomization (Joseph, Beavers & Funada 2002; Theofanous 2011). In the hemline breakup mode, the high-velocity air skims over the gel drops, and the edges of the drops constantly deform into thin membranes. The drop core also deforms into membranes and, eventually, all these membranes break up into reticular fragments. The hemline breakup of gels and the sheet-thinning breakup of Newtonian fluids are similar in some ways since their deformations all start from the edges of the drops. (Guildenbecher *et al.* 2009; Jackiw & Ashgriz 2021) Therefore, the hemline breakup may be related to the shear instability at the edges of the drops, which is identical to the sheet-thinning breakup of Newtonian fluids.

We performed comparative experiments to verify whether this unique hemline breakup is affected by viscosity. We used maltose syrup as the working fluid instead of pure water because the viscosity of pure water is too low. The secondary breakup process of maltose syrup is shown in figure 10. The drops exhibit multimode breakup and sheet-thinning breakup sequentially as the air-flow velocity increases. It is indicated that the breakup morphologies of maltose syrup are identical to those of Newtonian fluids. Compared with many previous studies, it can be found that there is no hemline breakup in the secondary breakup of viscous fluids. As discussed in § 3.1, the elasticity of the gel with $\varphi = 0.5\,\%$ is too small to be measured, which means it can be considered negligible. The elasticity of the gel increases with increasing concentration; however, according to the experimental results, gel drops with $\varphi = 0.5\,\%$–$1.5\,\%$ all exhibited hemline breakup in the secondary breakup process. In other words, gel drops with $\varphi = 0.5\,\%$ still exhibited hemline breakup, even if their elasticity was negligible. Considering the similarity between the hemline breakup of gel drops and the sheet-thinning breakup of Newtonian fluids, it is suggested that the hemline breakup occurs based on the influence of viscosity on the sheet-thinning breakup mode, and the yield stress further affects the breakup morphology, which leads to the appearance of the hemline breakup.

The breakup mode classification of guar gum gel drops and the relation of the transitional *We* and *Oh* are plotted in figure 11. As proposed by Brodkey (1967) and Pilch & Erdman (1987), the correlation of the critical Weber number, We_c, and the Ohnesorge number, Oh, is $We_c = We_{cOh\to 0}(1 + 1.077Oh^{1.6})$. Here, $We_{cOh\to 0}$ is the critical *We* at low Oh. As they suggested, We_c between the deformation and the bag breakup is

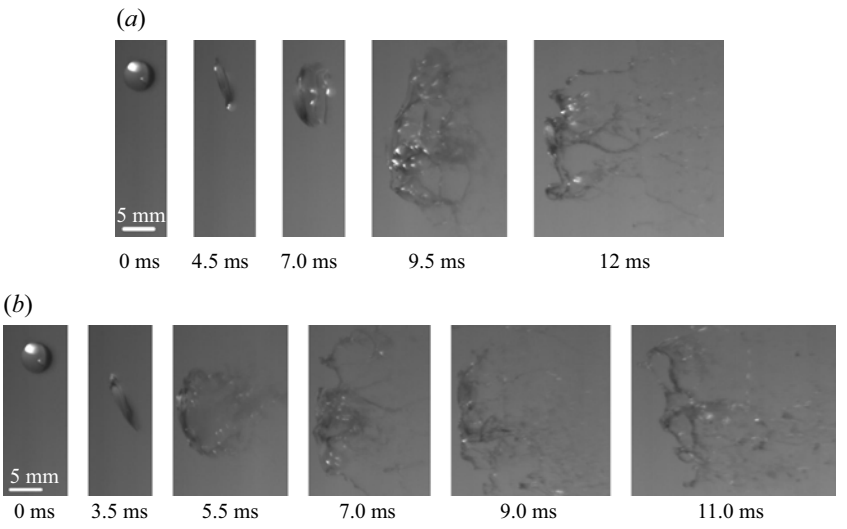

Figure 10. Secondary breakup of the maltose syrup; the air flows from left to right: (*a*) multimode breakup of $\varphi = 70\,\%$, $u_g = 45.9\,\mathrm{m\,s^{-1}}$, $We = 256.0$, $Oh = 1.1$; (*b*) sheet-thinning breakup of $\varphi = 70\,\%$, $u_g = 61.2\,\mathrm{m\,s^{-1}}$, $We = 460.4$, $Oh = 1.1$.

approximately $We_{cOh\to 0} = 11$, and We_c of the sheet-thinning breakup is approximately $We_{cOh\to 0} = 80$. On this basis, we fitted the data of our experiments to obtain (3.8) and (3.9). The correlation We_1 represents the transition between the deformation and bag-and-stamen breakup, which is

$$\begin{aligned} We_1 &= 11(1 + 2.4Oh^{1.3}) \\ &= 11\left(1 + 2.4\left(\frac{1}{\phi}\frac{\tau_0 D_0}{\sigma}\sqrt{\frac{\rho_g}{\rho_l We}} + \frac{K\left(\phi\dfrac{u_g}{D_0}\right)^{n-1}}{(\rho_l D_0\sigma)^{1/2}}\right)^{1.3}\right), \end{aligned} \tag{3.8}$$

where the fitting correlation coefficient is 0.98. The correlation We_2 represents the transition between the bag-and-stamen breakup and the hemline breakup, which is

$$\begin{aligned} We_2 &= 80(1 + 2.4Oh^{1.3}) \\ &= 80\left(1 + 2.4\left(\frac{1}{\phi}\frac{\tau_0 D_0}{\sigma}\sqrt{\frac{\rho_g}{\rho_l We}} + \frac{K\left(\phi\dfrac{u_g}{D_0}\right)^{n-1}}{(\rho_l D_0\sigma)^{1/2}}\right)^{1.3}\right), \end{aligned} \tag{3.9}$$

where the fitting correlation coefficient is 0.99. The Oh value indicates the effect of viscosity in classifying the critical conditions for different breakup modes. The velocity of the air-flow field and the shear rate are correspondingly high. The gel shows a shear-thinning behaviour ($n < 1$) under such a high shear rate; and the viscosity of the gel is small at this time. Therefore, the exponent in the correlation is 1.3, which is lower than that in the correlation proposed by Brodkey (1967) Combining equations (3.8) and

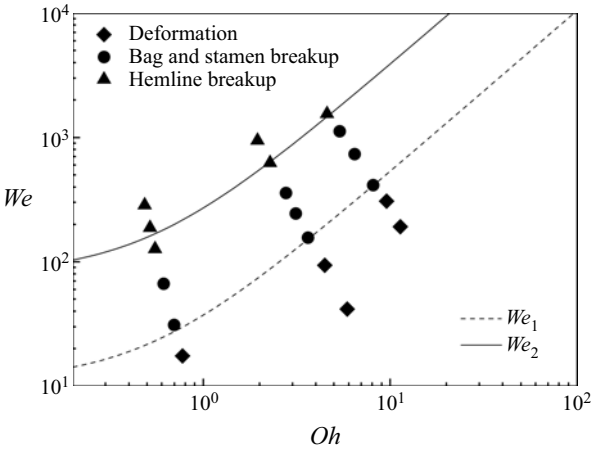

Figure 11. The breakup regime of guar gum gel drops.

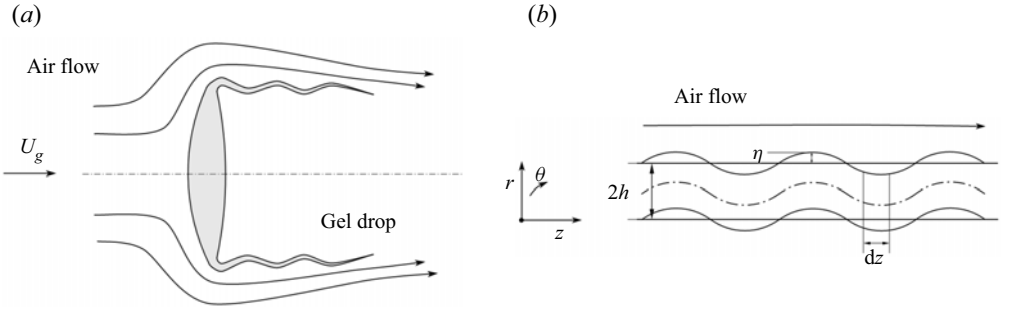

Figure 12. (*a*) The breakup mechanism of hemline breakup; (*b*) schematic diagram of an antisymmetric disturbance of a liquid sheet.

(3.9) and the experimental results of the breakup morphologies, the hemline breakup is indeed a modified behaviour of the sheet-thinning breakup. As a modification term for *Oh*, the effect of yield stress on the classification of different breakup modes is also shown in (3.8) and (3.9). Detailed analysis of the yield stress is discussed in § 3.4.

3.4. *Discussion on formation and breakup of gel membranes*

As observed in the hemline breakup mode, the edge of the gel drops continuously generated a large number of membranes. Instead of breaking up into filaments or tiny droplets, these gel membranes stabilize and remain intact until the drop core also deforms into membranes. The final breakup of the gel drops is manifested by the fragmentation of the bulk gel membranes. Under the combined effects of aerodynamic, surface tension, inertial and viscous forces, the gel membranes destabilize and eventually break up. Dombrowski & Johns (1963) investigated the linear stability analysis of a liquid sheet with a constant velocity travelling through a stationary gas. They indicated that the final breakup of the liquid sheet is dominated by the unstable disturbance of maximum growth rate. Inspired by their study, we drew on a similar analytical method to explore the destabilization and breakup of gel membranes, thereby explaining the novel phenomenon in the hemline breakup mode.

The breakup mechanism of hemline breakup is shown in figure 12(*a*). On this basis, we established a columnar coordinate system and explored the antisymmetric disturbance of a viscous liquid sheet in the air flow with velocity U_g. The schematic diagram is shown in figure 12(*b*). The thickness of the viscous liquid sheet is $2h$. The aerodynamic force $\mathrm{d}F_P$ caused by the air flow is

$$\mathrm{d}F_P = 2k\rho_g U_g^2 r^2\theta\,\mathrm{d}z, \tag{3.10}$$

where the k is the wavenumber. The force $\mathrm{d}F_\sigma$ caused by surface tension σ is

$$\mathrm{d}F_\sigma = \frac{\partial}{\partial z}\left(2\sigma r\theta\frac{\partial r}{\partial z}\right)\mathrm{d}z = 2\sigma r\theta\frac{\partial^2 r}{\partial z^2}\,\mathrm{d}z. \tag{3.11}$$

The gel membranes fluctuate under the disturbance, and the change of momentum leads to the inertial force $\mathrm{d}F_I$, which is

$$\mathrm{d}F_I = -\frac{\partial}{\partial t}\left(\rho_l r\theta h\,\mathrm{d}z\frac{\partial r}{\partial t}\right) = -\rho_l\left(\frac{\partial h}{\partial t}\frac{\partial r}{\partial t} + h\frac{\partial^2 r}{\partial t^2}\right)r\theta\,\mathrm{d}z = -\rho_l r\theta h\frac{\partial^2 r}{\partial t^2}\,\mathrm{d}z. \tag{3.12}$$

We assumed that the thickness of the liquid sheet is changeless with time, which means $\partial h/\partial t = 0$. For a Herschel–Bulkley liquid as in (3.3), the shear stress τ consists of viscous force τ_μ and yield stress τ_0. Therefore, the viscous force $\mathrm{d}F_\mu$ is

$$\begin{aligned}\mathrm{d}F_\mu &= \frac{\partial}{\partial z}(\tau_\mu r\theta h)\,\mathrm{d}z = \left(h\frac{\partial\tau_\mu}{\partial z} + \frac{\partial t}{\partial z}\frac{\partial h}{\partial t}\frac{\partial^2 r}{\partial t\partial z}\right)r\theta\,\mathrm{d}z \\ &= \left(h\frac{\partial\tau_\mu}{\partial z} + \frac{1}{U_g}\frac{\partial h}{\partial t}\frac{\partial^2 r}{\partial t\partial z}\right)r\theta\,\mathrm{d}z = h\frac{\partial\tau_\mu}{\partial z}r\theta\,\mathrm{d}z.\end{aligned} \tag{3.13}$$

In the z-direction, the yield stress is

$$\mathrm{d}F_{\tau_0} = -2k\tau_0 r^2\theta\,\mathrm{d}z. \tag{3.14}$$

Therefore, the destabilization and breakup of liquid sheet occurs when the total force is $\mathrm{d}F > 0$, and the critical condition is

$$\begin{aligned}\mathrm{d}F = \mathrm{d}F_P + \mathrm{d}F_\sigma + \mathrm{d}F_I + \mathrm{d}F_\mu + \mathrm{d}F_{\tau_0} &= 2k\rho_g U_g^2 r^2\theta\,\mathrm{d}z \\ + 2\sigma r\theta\frac{\partial^2 r}{\partial z^2}\,\mathrm{d}z - \rho_l r\theta h\frac{\partial^2 r}{\partial t^2}\,\mathrm{d}z + h\frac{\partial\tau_\mu}{\partial z}r\theta\,\mathrm{d}z - 2k\tau_0 r^2\theta\,\mathrm{d}z &= 0,\end{aligned} \tag{3.15}$$

i.e.

$$2k\rho_g U_g^2 r + 2\sigma\frac{\partial^2 r}{\partial z^2} - \rho_l h\frac{\partial^2 r}{\partial t^2} + h\frac{\partial\tau_\mu}{\partial z} - 2k\tau_0 r = 0. \tag{3.16}$$

The antisymmetric disturbance is described by a sinusoidal wave as

$$r = \eta\sin(kz + \varepsilon), \tag{3.17}$$

where the η represents the amplitude and is a function of time

$$\eta = \eta_0\exp[\mathrm{i}(kz - \omega t)], \tag{3.18}$$

where η_0 is the initial amplitude; $\omega = \omega_r + \mathrm{i}\omega_i$ and the ω_r and ω_i are the frequency and growth rate of the disturbance. By inserting the derivative of (3.17) and (3.18) into (3.16) and plugging $\Omega_i = \omega_i h/U_g$, the Reynolds number $Re = \rho_l U_g h/\mu$ and the Weber number

$We = \rho_g U_g^2 h/\sigma$ into it, the equation is transformed to the dimensionless form. The final dispersion relation for a viscous liquid with yield stress is

$$\Omega_i^2 + \frac{(kh)^2}{Re}\Omega_i + 2(kh)^2\left(\frac{\tau_0}{\rho_g U_g^2}\frac{Q}{kh} + \frac{1}{We} - \frac{Q}{kh}\right) = 0, \tag{3.19}$$

where $Q = \rho_g/\rho_l$. Chojnacki & Feikema (1997) studied the breakup of a power-law liquid sheet and established its dispersion relation. When taking the yield stress into consideration, the dispersion relation for a gel is

$$\Omega_i^2 + n\frac{(kh)^2}{Re}\Omega_i^{2n-1} + 2(kh)^2\left(\frac{\tau_0}{\rho_g U_g^2}\frac{Q}{kh} + \frac{1}{We} - \frac{Q}{kh}\right) = 0, \tag{3.20}$$

where $Re = \rho_l U_g h/\mu = \rho_l U_g^{2-n} h^n/K$.

In the studies of Chojnacki & Feikema (1997) and Yang *et al.* (2012) on the breakup of a power-law liquid sheet, it is indicated via theoretical derivation and exploration that the increase in the consistency coefficient K and the fluid behaviour index n leads to a decrease of the maximum growth rate and dominant wavenumber. In our experiments, the Herschel–Bulkley rheological model as in (3.3) is used to describe the yield stress and shear-thinning behaviour of the gel. The third term in (3.20) represents the effect of yield stress on the breakup of a gel membrane. Compared with a Newtonian fluid or a power-law fluid, the yield stress of a gel leads to a decrease in the maximum growth rate and dominant wavenumber. In other words, the yield stress restrains the growth of disturbance waves. Some of the gel membranes remain intact rather than breaking into filaments in the hemline breakup mode, which may be related to the competition between the yield stress and the aerodynamic force. Zhao *et al.* (2011*b*) investigated the secondary breakup of coal water slurry and proposed a dimensionless number to describe this competition. Here, we quote the reciprocal form of this dimensionless number and define it as C_y:

$$C_y = \frac{\tau_0}{\rho_g U_g^2}. \tag{3.21}$$

Then (3.20) will be

$$\Omega_i^2 + n\frac{(kh)^2}{Re}\Omega_i^{2n-1} + 2C_y khQ + \frac{2(kh)^2}{We} - 2khQ = 0. \tag{3.22}$$

For a Newtonian fluid or a power-law fluid, the third term in (3.22) equals zero, which means the breakup of the liquid sheet is governed by the other four forces. For a gel whose yield stress has an obvious effect on the breakup of the liquid sheet, the third term leads to the decrease of the maximum growth rate and dominant wavenumber. We solved (3.22) under different initial conditions. The relation between the dimensionless wavenumber $k \times h$ and the dimensionless growth rate of disturbance wave Ω_i is shown in the figure 13. By increasing τ_0 from 0 to 100 Pa, the influence of yield stress τ_0 on the development of a disturbance wave in Newtonian fluids and shear-thinning fluids is studied. According to the results, the yield stress τ_0 inhibits the growth of the disturbance wave. Therefore, the maximum growth rate and the dominant wavenumber decrease with the increase of yield stress τ_0. Therefore, the gel sheet tends to perform the long wave breakup mode because of the decrease in the maximum growth rate and the dominant wavenumber, which explains

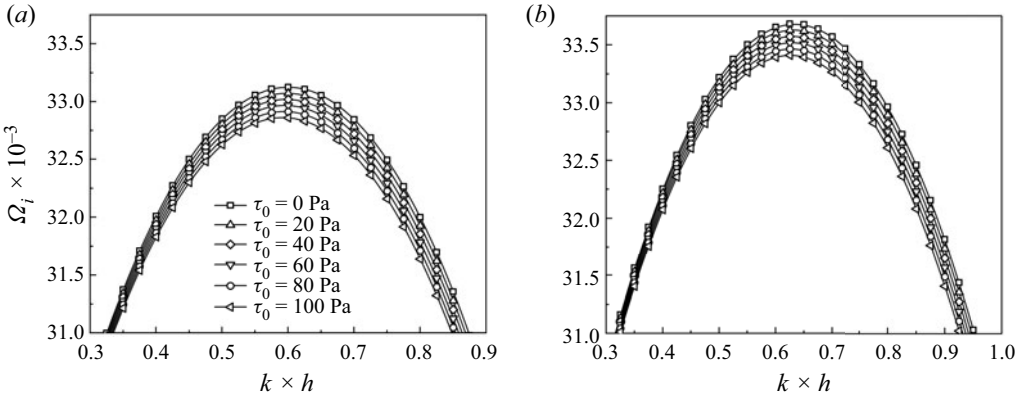

Figure 13. Effect of yield stress on stability of gel membrane: (*a*) $n = 0.35$, $K = 10.0$ Pa s^n, $2h = 0.1$ mm, $u_g = 76.5$ m s^{-1}, $Re = 7298.5$; (*b*) $n = 1$, $K = 10.0$ Pa s^n, $2h = 0.1$ mm, $u_g = 76.5$ m s^{-1}, $Re = 7298.5$.

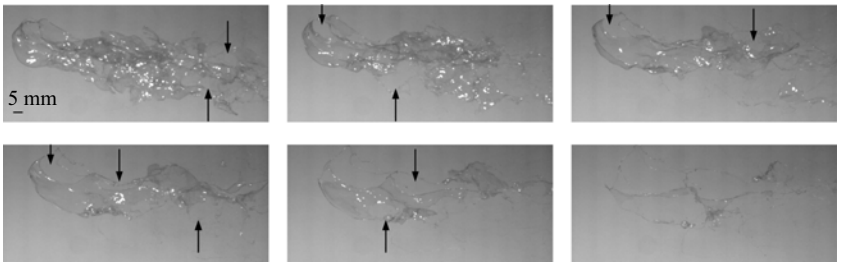

$\varphi = 1.0\,\%$ $u_g = 76.5$ m s^{-1}, $\Delta t = 1.0$ ms

Figure 14. Reticular breakup of a gel membrane, the arrows point to the breaking points.

that fact that the gel membranes formed in the hemline breakup mode remain intact instead of breaking into filaments.

Based on this, Oh in (3.5) can be rewritten by inserting C_y, which is

$$Oh = \frac{\mu_l}{(\rho_l D_0 \sigma)^{1/2}} = \frac{\tau_0 + K\left(\phi \frac{u_g}{D_0}\right)^n}{\phi u_g \left(\frac{\rho_l \sigma}{D_0}\right)^{1/2}} = \frac{1}{\phi} C_y \sqrt{\frac{\rho_g}{\rho_l} We} + \frac{K\left(\phi \frac{u_g}{D_0}\right)^{n-1}}{(\rho_l D_0 \sigma)^{1/2}}. \tag{3.23}$$

Therefore, (3.7)–(3.9) contain the effect of yield stress on breakup time and breakup mode classification, respectively; Oh increases when C_y increases, leading to a longer breakup time and a change in the breakup mode, which means that, as an addition item of viscosity, the yield stress delays the breakup of gel drops.

The intact gel membranes exhibit flexural vibration and exhibit reticular breakup, as shown in figure 14. It can be observed that the breaking points of the membranes occur at high amplitudes where the rest of the membranes remain, leading to the formation of reticular fragments. The flow field around the droplet is studied by Flock *et al.* (2012) and Kant & Banerjee (2022) through experiments and simulations. The recirculation zone of air around the droplet generates high negative pressure downstream. As a result, the droplets deform and break up when the vortices shed into the air-flow wake. However, the air-flow-wake structure is unlikely to dominate the breakup morphology of the droplets. In our experiments, the shedding vortices may affect the reticular breakup of

the gel membrane. The mechanism of this effect is unknown to us at present and will perhaps be investigated in future work.

4. Conclusion

We measured the rheological properties of guar gum gels by a rotational rheometer. The secondary breakup process of the gel drops was observed by a high-speed camera. It is indicated that the yield stress of gels has a significate effect on the breakup morphology.

The secondary breakup of the gels can be classified into three modes: deformation, bag type and hemline type. The deformation regime appears when the air velocity is low, where the aerodynamic force is too small to dominate, leading to the absence of drop breakup. When the air velocity slightly increases, the gel drops exhibit the bag-type breakup. A spherical drop flattens and deforms into a bag-like structure, such as bag type or stamen type.

Combining breakup morphologies and the regime map, the hemline breakup is indeed a modified behaviour of the sheet-thinning breakup. Gel drops enter the hemline breakup mode with increasing air velocity. As the high-velocity air skims over the gel drops, the edges of the drops constantly deform into thin membranes until the drop core eventually deforms into membranes as well. These membranes vibrate vertically at different positions. Breaking points occur at high amplitudes and form reticular fragments. A linear stability analysis is investigated to explore the phenomenon in hemline breakup mode. The dimensionless number $C_y = \tau_0/\rho_g U_g^2$ is proposed to describe the relative magnitude of yield stress and aerodynamic force. The results show that the yield stress of the gel drops leads to a decrease in the maximum growth rate and dominant wavenumber at the edges of the drops. The formation of the gel membranes is considered to be related to the effect of yield stress that further modifies the effect of viscosity. Gels with higher yield stress have higher resistance to deformation, resulting in longer breakup times. The breakup regime map of gel drop is also proposed based on *We* and *Oh*.

Funding. This research was supported by the National Natural Science Foundation of China (U21B2088).

Declaration of interests. The authors report no conflict of interest.

Author ORCIDs.
Hui Zhao https://orcid.org/0000-0002-8379-0399;
Hai-Feng Liu https://orcid.org/0000-0002-2572-8693.

References

Beckers, D., Ellendt, N., Fritsching, U. & Uhlenwinkel, V. 2020 Impact of process flow conditions on particle morphology in metal powder production via gas atomization. *Adv. Powder Technol.* **31** (1), 300–311.

Brodkey, R.S. 1967 *The Phenomena of Fluid Motions*. Addison-Wesley.

Cao, Y. & Mezzenga, R. 2020 Design principles of food gels. *Nat. Food* **1** (2), 106–118.

Chojnacki, K. & Feikema, D. 1997 Study of non-Newtonian liquid sheets formed by impinging jets. In *Paper read at 33rd Joint Propulsion Conference and Exhibit*.

Chu, G., Qian, L., Zhong, X., Zhu, C. & Chen, Z. 2020 A numerical investigation on droplet bag breakup behavior of polymer solution. *Polymers* **12** (10), 2172.

Dai, Z. & Faeth, G.M. 2001 Temporal properties of secondary drop breakup in the multimode breakup regime. *Intl J. Multiphase Flow* **27** (2), 217–236.

Daly, A.C., Riley, L., Segura, T. & Burdick, J.A. 2020 Hydrogel microparticles for biomedical applications. *Nat. Rev. Mater.* **5** (1), 20–43.

Dombrowski, N. & Johns, W.R. 1963 The aerodynamic instability and disintegration of viscous liquid sheets. *Chem. Engng Sci.* **18** (3), 203–214.

EGGERS, J. & VILLERMAUX, E. 2008 Physics of liquid jets. *Rep. Prog. Phys.* **71** (3), 036601.
FLOCK, A.K., GUILDENBECHER, D.R., CHEN, J., SOJKA, P.E. & BAUER, H.J. 2012 Experimental statistics of droplet trajectory and air flow during aerodynamic fragmentation of liquid drops. *Intl J. Multiphase Flow* **47**, 37–49.
GELFAND, B.E. 1996 Droplet breakup phenomena in flows with velocity lag. *Prog. Energy Combust. Sci.* **22** (3), 201–265.
GLUSHKOV, D.O., PAUSHKINA, K.K., PLESHKO, A.O. & VYSOKOMORNY, V.S. 2022 Characteristics of micro-explosive dispersion of gel fuel particles ignited in a high-temperature air medium. *Fuel* **313**, 123024.
GLUSHKOV, D.O., PLESHKO, A.O. & YASHUTINA, O.S. 2020 Influence of heating intensity and size of gel fuel droplets on ignition characteristics. *Intl J. Heat Mass Transfer* **156**, 119895.
GUILDENBECHER, D.R., LÓPEZ-RIVERA, C. & SOJKA, P.E. 2009 Secondary atomization. *Exp. Fluids* **46** (3), 371.
HOANG, A.T. 2021 Combustion behavior, performance and emission characteristics of diesel engine fuelled with biodiesel containing cerium oxide nanoparticles: a review. *Fuel Process. Technol.* **218**, 106840.
HSIANG, L.P. & FAETH, G.M. 1995 Drop deformation and breakup due to shock wave and steady disturbances. *Intl J. Multiphase Flow* **21** (4), 545–560.
JACKIW, I.M. & ASHGRIZ, N. 2021 On aerodynamic droplet breakup. *J. Fluid Mech.* **913**, A33.
JIAO, D., ZHANG, F., DU, Q., NIU, Z. & JIAO, K. 2017 Direct numerical simulation of near nozzle diesel jet evolution with full temporal-spatial turbulence inlet profile. *Fuel* **207**, 22–32.
JOSEPH, D.D., BEAVERS, G.S. & FUNADA, T. 2002 Rayleigh–Taylor instability of viscoelastic drops at high Weber numbers. *J. Fluid Mech.* **453**, 109–132.
KANT, K. & BANERJEE, R. 2022 Study of the secondary droplet breakup mechanism and regime map of Newtonian and power law fluids at high liquid–gas density ratio. *Phys. Fluids* **34** (4), 043108.
KÉKESI, T., AMBERG, G. & PRAHL WITTBERG, L. 2014 Drop deformation and breakup. *Intl J. Multiphase Flow* **66**, 1–10.
KÉKESI, T., AMBERG, G. & PRAHL WITTBERG, L. 2016 Drop deformation and breakup in flows with shear. *Chem. Engng Sci.* **140**, 319–329.
KULKARNI, V. & SOJKA, P.E. 2014 Bag breakup of low viscosity drops in the presence of a continuous air jet. *Phys. Fluids* **26** (7), 072103.
MINAKOV, A.V., SHEBELEVA, A.A., STRIZHAK, P.A., CHERNETSKIY, M.Y. & VOLKOV, R.S. 2019 Study of the Weber number impact on secondary breakup of droplets of coal water slurries containing petrochemicals. *Fuel* **254**, 115606.
NARAYANASWAMY, R. & TORCHILIN, V.P. 2019 Hydrogels and their applications in targeted drug delivery. *Molecules* **24** (3), 603.
DE OLIVEIRA, P.M., MESQUITA, L.C.C., GKANTONAS, S., GIUSTI, A. & MASTORAKOS, E. 2021 Evolution of spray and aerosol from respiratory releases: theoretical estimates for insight on viral transmission. *Proc. R. Soc.* A*: Math. Phys. Engng Sci.* **477** (2245), 20200584.
PADWAL, M.B., NATAN, B. & MISHRA, D.P. 2021 Gel propellants. *Prog. Energy Combust.* **83**, 100885.
PILCH, M. & ERDMAN, C.A. 1987 Use of breakup time data and velocity history data to predict the maximum size of stable fragments for acceleration-induced breakup of a liquid drop. *Intl J. Multiphase Flow* **13** (6), 741–757.
QIAN, L., ZHONG, X., ZHU, C. & LIN, J. 2021 An experimental investigation on the secondary breakup of carboxymethyl cellulose droplets. *Intl J. Multiphase Flow* **136**, 103526.
RIMBERT, N., CASTRILLON ESCOBAR, S., MEIGNEN, R., HADJ-ACHOUR, M. & GRADECK, M. 2020 Spheroidal droplet deformation, oscillation and breakup in uniform outer flow. *J. Fluid Mech.* **904**, A15.
SHARMA, S., PINTO, R., SAHA, A., CHAUDHURI, S. & BASU, S. 2021 On secondary atomization and blockage of surrogate cough droplets in single- and multilayer face masks. *Sci. Adv.* **7** (10), eabf0452.
THEOFANOUS, T.G. 2011 Aerobreakup of Newtonian and viscoelastic liquids. *Annu. Rev. Fluid Mech.* **43**, 661–690.
THEOFANOUS, T.G. & LI, G.J. 2008 On the physics of aerobreakup. *Phys. Fluids* **20** (5), 052103.
THEOFANOUS, T.G., MITKIN, V.V., NG, C.L., CHANG, C.-H., DENG, X. & SUSHCHIKH, S. 2012 The physics of aerobreakup. II. Viscous liquids. *Phys. Fluids* **24** (2), 022104.
TUAN HOANG, A. & VIET PHAM, V. 2021 2-Methylfuran (MF) as a potential biofuel: a thorough review on the production pathway from biomass, combustion progress, and application in engines. *Renew. Sustain. Energy Rev.* **148**, 111265.
WEI, M., CHEN, S., SUN, M., LIANG, J., LIU, C. & WANG, M. 2020 Atomization simulation and preparation of 24CrNiMoY alloy steel powder using VIGA technology at high gas pressure. *Powder Technol.* **367**, 724–739.

WU, H., ZHANG, F. & ZHANG, Z. 2021 Fundamental spray characteristics of air-assisted injection system using aviation kerosene. *Fuel* **286**, 119420.

YANG, L.-J., FU, Q.-F., QU, Y.-Y., GU, B. & ZHANG, M.-Z. 2012 Breakup of a power-law liquid sheet formed by an impinging jet injector. *Intl J. Multiphase Flow* **39**, 37–44.

YANG, W., JIA, M., CHE, Z., SUN, K. & WANG, T. 2017 Transitions of deformation to bag breakup and bag to bag-stamen breakup for droplets subjected to a continuous gas flow. *Intl J. Heat Mass Transfer* **111**, 884–894.

YANG, W., JIA, M., SUN, K. & WANG, T. 2016 Influence of density ratio on the secondary atomization of liquid droplets under highly unstable conditions. *Fuel* **174**, 25–35.

ZHAO, H., HOU, Y.-B., LIU, H.-F., TIAN, X.-S., XU, J.-L., LI, W.-F., LIU, Y., WU, F.-Y., ZHANG, J. & LIN, K.-F. 2014 Influence of rheological properties on air-blast atomization of coal water slurry. *J. Non-Newtonian Fluid Mech.* **211**, 1–15.

ZHAO, H., LIU, H.-F., CAO, X.-K., LI, W.-F. & XU, J.-L. 2011*a* Breakup characteristics of liquid drops in bag regime by a continuous and uniform air jet flow. *Intl J. Multiphase Flow* **37** (5), 530–534.

ZHAO, H., LIU, H.-F., LI, W.-F. & XU, J.-L. 2010 Morphological classification of low viscosity drop bag breakup in a continuous air jet stream. *Phys. Fluids* **22** (11), 114103.

ZHAO, H., LIU, H.-F., XU, J.-L. & LI, W.-F. 2011*b* Secondary breakup of coal water slurry drops. *Phys. Fluids* **23** (11), 113101.

ZHU, W., ZHAO, N., JIA, X., CHEN, X. & ZHENG, H. 2021 Effect of airflow pressure on the droplet breakup in the shear breakup regime. *Phys. Fluids* **33** (5), 053309.